Polyoxometalates

Deutsche Ausgabe: DOI: 10.1002/ange.201607151
Internationale Ausgabe: DOI: 10.1002/anie.201607151

Closing Uranyl Polyoxometalate Capsules with Bismuth and Lead Polyoxocations

*Olivier Renier, Clément Falaise, Harrison Neal, Karoly Kozma, and May Nyman**

Abstract: *Uranyl polyoxometalate clusters are both fundamentally fascinating and potentially relevant to nuclear energy applications. With only ten years of development, there is still much to be discovered about heterometal derivatives and aqueous speciation and behavior. Herein, we show that it is possible to encapsulate the polyoxocations $[Bi_6O_8]^{2+}$ and $[Pb_8O_6]^{4+}$ in $[(UO_2)(O_2)(OH)]_{24}^{24-}$ (denoted $Bi@U_{24}$ and $Pb@U_{24}$) in pure form and high yields despite the fact that under aqueous conditions, these compounds are stable on opposite ends of the pH scale. Moreover, $[Pb_8O_6]^{4+}$ is a formerly unknown Pb^{II} polynuclear species, both in solution and in the solid state. Raman spectroscopic and mass spectrometric analysis of the reaction solutions revealed the very rapid assembly of the nested clusters, driven by bismuth- or lead-promoted decomposition of excess peroxide, which inhibits U_{24} formation. Experimental and simulated small-angle X-ray scattering data of $Bi@U_{24}$ and $Pb@U_{24}$ solutions revealed that this technique is very sensitive not only to the size and shape of the clusters, but also to the encapsulated species.*

Researchers have engaged in polyoxometalate (POM) chemistry for decades, motivated by their aesthetic structural diversity and exploitable properties as solids, in solutions, and on surfaces.[1] POMs have found application in redox reactions, acid–base chemistry, colorimetric assays, inorganic ligation, and supramolecular assembly in both solution and the solid phase.[2] Classic POMs are Group V and VI polyanions in their highest oxidation state with a terminal and inert "yl" oxo group, which stabilizes the molecular form in water. In 2005, Burns[3] and co-workers demonstrated that the aqueous uranyl cation (UO_2^{2+}), which has two *trans* yl oxo groups, can assemble into large discrete polyanionic capsules through the formation of peroxide bridges. Oxo ligands terminate both the exterior and the interior of the capsule. Since this first report, over 50 capsule geometries containing up to 124 uranyl building units have been described.[4] Capsules featuring 24, 28, 32, and 60 uranyl polyhedra have received the most attention in studies of growth mechanisms, supramolecular assembly, solution-phase behavior, and compositional variation of the encapsulated species.[5] Furthermore, recent studies implied the utility of uranyl capsules in different steps of the nuclear fuel cycle (e.g., separation, enrichment, and fuel fabrication).[6] Most commonly, these capsules assemble in alkaline peroxidic solutions, and both the pH and the counterions (mainly alkali metal cations) have key roles in determining cluster geometry.[5d,7] There have only been a few reports[6b] that feature encapsulated metal cations other than alkali metal ions, mainly owing to the challenges associated with controlling the speciation and solubility of most metal cations in basic media.

Herein, we show that uranyl nanocages can also encapsulate heavy p-block polyoxocations, namely $[Bi_6O_8]^{2+}$ and $[Pb_8O_6]^{4+}$, yielding $Bi@U_{24}$ and $Pb@U_{24}$. Despite the challenges associated with the incompatibility of uranyl and p-block clusters under aqueous conditions, these species were isolated in high yields, enabling detailed solution characterization of the assembly process and the crystalline products. The $[Bi_6O_8]^{2+}$ hexamer has previously been characterized in solution and in the solid state,[8] but the $[Pb_8O_6]^{4+}$ octamer had not been described thus far. We have recently demonstrated the unique ability of small-angle X-ray scattering (SAXS) to distinguish capsule geometries and sizes in solution without crystallization of the dominant species.[5d] This is owed to the distinctive oscillations in the scattering data that are especially characteristic of core–shell structures. Herein, we demonstrate through "filling" the core with metals that possess electron density more comparable to that of uranium that SAXS can also distinguish the content of these capsules.

$Bi@U_{24}$ was synthesized from $Li_4[UO_2(O_2)_3]\cdot x\,H_2O$ monomer, bismuth nitrate, and nitric acid in water with a Bi/U ratio of 1:4 (see the Supporting Information for details). After nearly complete evaporation of this solution (pH 12.3), clear yellow crystals were obtained in 70 % yield. Likewise, $Pb@U_{24}$ was prepared from a 1:3 Pb/U mixture ($Li_4[UO_2(O_2)_3]\cdot x\,H_2O$ and lead nitrate; pH 12.5) in 90 % yield. $Bi@U_{24}$ and $Pb@U_{24}$ were both synthesized by a one-pot approach in alkaline solution. The reaction solution is alkaline because the peroxide ligands of the $[UO_2(O_2)_3]^{4-}$ monomer are protonated upon dissolution in water. It is not surprising that the initial reaction solutions are cloudy, and the formation of the nested clusters probably involves reaction at the precipitate–solution interface. Bismuth nitrate is extremely insoluble in water except at very low pH values, a property exploited in medicinal applications, and the same is true for lead(II). The aqueous speciation of Bi^{3+} [8d] has been investigated; above pH ≈ 1.5, it hydrolyzes to the insoluble hexameric form that is encapsulated in $Bi@U_{24}$. For this reason, it is remarkable that the $Bi@U_{24}$ and $Pb@U_{24}$ reaction solutions (see the Supporting Information, Figure S1) are transparent and nearly transparent, respectively, upon completion of the self-assembly process, and that the reactions give $Bi@U_{24}$ and $Pb@U_{24}$ in high yields at pH > 12. X-ray scattering analysis of

[*] O. Renier, Dr. C. Falaise, H. Neal, K. Kozma, Prof. Dr. M. Nyman
Department of Chemistry, Oregon State University
Corvallis, Oregon 97331-4003 (USA)
E-mail: may.nyman@oregonstate.edu

Supporting information and the ORCID identification number(s) for the author(s) of this article can be found under: http://dx.doi.org/10.1002/anie.201607151.

fresh reaction solutions revealed polydisperse, large aggregates, likely composed of the p-block cluster (Figure S2). Based on this observation and the SAXS data, we suggest that $[Bi_6O_8]^{2+}$ and $[Pb_8O_6]^{4+}$ have been formed and precipitated immediately upon contact with the alkaline uranyl triperoxide solution. Their solubilization is enabled only by subsequent self-assembly of soluble U_{24}, encapsulating insoluble $[Bi_6O_8]^{2+}$ or $[Pb_8O_6]^{4+}$. The formation of $Bi@U_{24}$ and $Pb@U_{24}$ is more rapid than that of $Li@U_{24}$ because either 1) the Bi and Pb clusters act as templates for U_{24} assembly or 2) Bi and Pb aid in decomposing excess peroxide, which inhibits U_{24} formation.[5c] The dominant aqueous polynuclear form of Pb^{II} has long been described as Pb_6O_8,[9] but the presence of $[Pb_8O_6]^{4+}$ in $Pb@U_{24}$ suggests otherwise.

Crystal data and structural refinement information are summarized in Table S1, and the salient structural features are summarized in Figure 1. For $Bi@U_{24}$,[10] the six bismuth

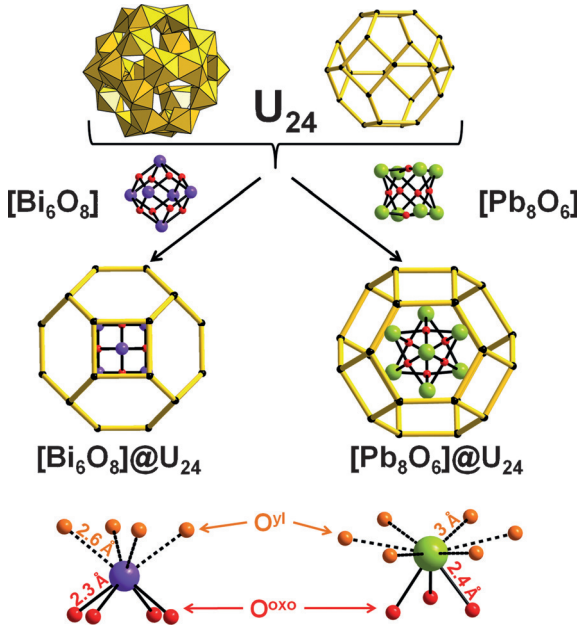

Figure 1. Views of $Bi@U_{24}$ and $Pb@U_{24}$. Uranyl is shown in yellow in polyhedral and wire-frame representation (black nodes are U^{6+}). The bismuth (purple) atoms are located in the square faces while the lead (green) atoms are located in the hexagonal faces.

centers form an ideal octahedral core, with adjacent Bi–Bi distances of about 3.8 Å. Each Bi^{3+} cation is linked to four other Bi^{3+} ions through four μ_3-oxo bridges (Bi–O ≈ 2.26 Å, BVS ≈ 0.6; Tables S2 and S3), defining the building unit $[Bi_6O_8]^{2+}$. Each bismuth cation is found in a pseudo square antiprismatic environment, defined by four μ_3-oxo units of $[Bi_6O_8]^{2+}$ and the four yl oxo groups of one square face of U_{24} (Figure 1). Each of the relatively short Bi–O^{yl} distances (2.6 Å) contributes 10% to the bond valence sum of Bi, indicating the participation of the yl oxo units in the coordination sphere of Bi^{3+}. This is an unusual example of heterometallic cation–cation interactions (CCIs; U=O–Bi). Cation–cation interactions are defined in the inorganic sense as a bond between a "metyl" and a second metal cation bridged through a multiply bonded oxo group. These usually involve d^0 POMs, diuranyl, or dineptunyl, and the interaction can be homometallic[11] or heterometallic.[12]

The U_{24} capsule has been described before.[3,5c,d] Briefly, it is composed of 24 $UO_2(O_2)_2(OH)_2$ polyhedra assembled into six square faces with peroxide bridges and eight hexagonal faces with alternating dihydroxide and peroxide bridges (Figure 1). The nesting of the bismuth hexamer into U_{24} provides a negatively charged supramolecular assembly, $\{Bi_6O_8 \subset [(UO_2)(O_2)(OH)]_{24}\}^{22-}$, charge-balanced with Li^+. The U/Bi ratio was confirmed by EDX analysis (obs: 4.3: calcd: 4.0; see the Supporting Information).

In $Bi@U_{24}$, the lone pair effect of the Bi^{3+} is weak, as indicated by the relatively short 2.6 Å interactions with the uranyl oxo groups. Thereby, part of our motivation to investigate Pb encapsulation was its stronger lone pair effect.[13] Single-crystal X-ray diffraction of $Pb@U_{24}$[14] revealed that the orientation of the encapsulated heavy metal cluster differs from that of $Bi@U_{24}$. Careful analysis of the X-ray data indicates that the Pb^{2+} cations are disordered over three positions (Figure 2): 1) in the plane defined by the

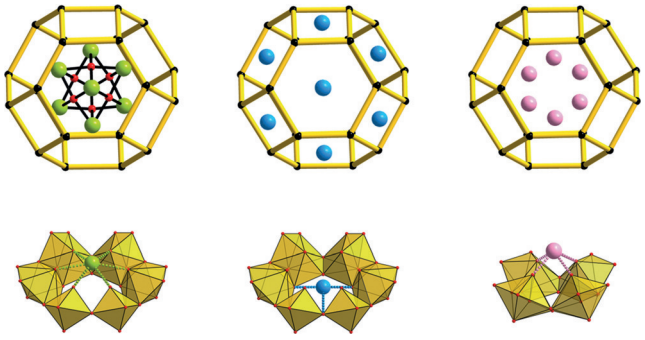

Figure 2. Illustration of the lead disorder observed in $Pb@U_{24}$. The lead sites in green, blue, and pink correspond to occupancies of 70, 20, and 10%, respectively.

six interior yl oxo groups of a hexagonal face of U_{24} (70% occupancy), 2) in the plane defined by six uranium centers of a hexagonal face (20% occupancy), and 3) associated with the four interior yl oxo groups of the square face (10% occupancy). These occupancies were determined by free refinement. The dominant Pb^{2+} type (70%) defines a previously unrecognized polycation, $[Pb_8O_6]^{4+}$ (Figure 1). These Pb^{2+} centers define the corners of a cube while the μ_4-oxo groups occupy the faces of the cube. (Pb–O ≈ 2.39 Å, BVS ≈ 0.47; Tables S4 and S5) The Pb^{2+} lone pairs point to the centers of the hexagonal faces with very long Pb–O^{yl} distances (Pb–O^{yl} ≈ 2.94 Å, BVS ≈ 0.1), indicating the very weak interaction of the Pb-based oxo cluster with the uranyl capsule, influenced by the stronger lone pair effect. These six Pb–O^{yl} bonds contribute 20% to the bond valence sum. Similar weak interactions of Pb with the yl oxo groups of uranyl cations have been observed in the mineral parsonsite ($Pb_2[UO_2(PO_4)_2]$).[15] The second lead site (20%) corresponds to the interaction of lead cations with three hydroxy ligands bridging uranyl centers within the hexagonal faces of the

capsule (Pb–OH ≈ 2.7 Å). Finally, the least occupied lead site (10%) is bonded to the four yl oxo groups of a square face with Pb–O^{yl} ≈ 2.4 Å and BVS ≈ 0.47. These cation–cation interactions of U=O–Pb are also observed in the mineral dumontite ($Pb_2[(UO_2)_3O_2(PO_4)_2]\cdot 5H_2O$).[16] EDX analysis confirmed the U/Pb ratio (obs: 2.87; calcd: 3.07; see the Supporting Information).

Although the charge-balancing lithium ions were not located crystallographically for either Bi@U_{24} or Pb@U_{24}, they were readily seen by ^{7}Li NMR spectroscopy upon dissolution in water (Figure S3). Additionally, a very small peak at −12 ppm was observed for Pb@U_{24}, which is consistent with encapsulated Li,[17] but shifted further downfield than previously observed. Both the larger chemical shift and the fact that this resonance is observed at all are consistent with co-encapsulation of Li and Pb. Owing to its high mobility, encapsulated Li could not be observed in the absence of non-mobile encapsulated species that slow down the exchange with Li in solution.[17]

To confirm the complex disorder of the encapsulated lead, solutions of redissolved Pb@U_{24} crystals were analyzed by ^{207}Pb NMR spectroscopy. The spectrum indeed revealed three broad resonances located at −413, −152, and 199 ppm (Figure 3); their integrated intensities are consistent with

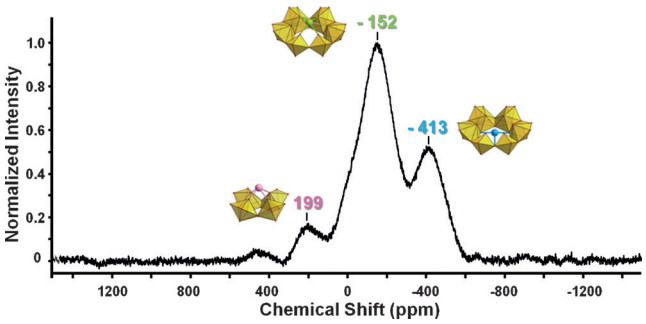

Figure 3. ^{207}Pb NMR spectra of dissolved crystals (in deionized water with 10% D_2O), illustrating the three different lead sites. The integrals are 0.30, 0.59, and 0.11 for the resonances at −413, −152, and 199 ppm, respectively.

the lead crystallographic sites. The substantial broadness of the resonances was attributed to the relative rigidity of the encapsulated Pb. Heating and in situ monitoring by ^{207}Pb NMR spectroscopy indicated minimal exchange amongst these sites (Figure S4).

Solutions of redissolved Bi@U_{24} and Pb@U_{24} crystals were then analyzed by SAXS. Experimental (Bi@U_{24} and Pb@U_{24}) and simulated (empty U_{24}, Bi@U_{24}, and Pb@U_{24}) scattering data are shown in Figure 4. The experimental and simulated scattering curves for Bi@U_{24} are nearly a perfect match, specifically in the Guinier region (q = 0.2–0.4 Å^{-1}), which determines the cluster radius of gyration, R_g (Table 1), and in terms of the positions and intensities of the first two oscillations (the third one is partially masked by solvent scattering). The first oscillation peaks are found at 0.73 Å^{-1} for both the calculated and experimental data and at 0.71 Å^{-1} for empty U_{24}. The diminished intensity of this first oscillation

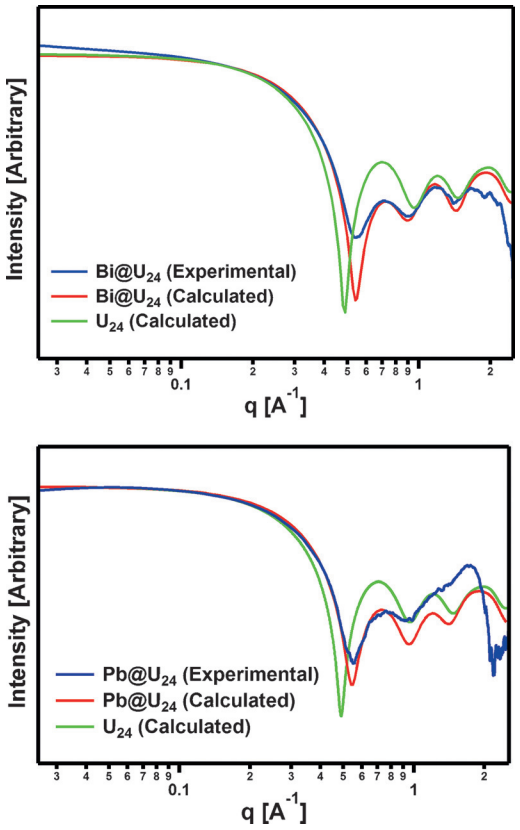

Figure 4. Comparison of the experimental and simulated scattering curves for Bi@U_{24} (top) and Pb@U_{24} (bottom) and the simulated scattering curve of the U_{24} shell.

Table 1: Core–shell electron densities[a] and radii of gyration (R_g) from the experimental X-ray scattering curves of M@U_{24} (M = Li, Bi, or Pb).

Capsule	ρ^{core} [b]	ρ^{shell} [b]	R_g [c]
Li@U_{24}	1.5	34.5	6.5
Bi@U_{24}	30.45	44.7	6.2
Pb@U_{24}	29.5	43.2	6.4

[a] Fixed parameters: shell thickness: 3.6 Å; core radius: 4.4 Å. [b] ρ = X-ray scattering length density (10^{10} cm^{-1}). [c] R_g is the shape-independent root mean square of the mass-weighted distances from the center of mass of a particle; for spherical particles, $R_s = \frac{\sqrt{5}}{3} R_g$.

for the filled capsule is characteristic of a high electron-density contrast between the core and shell for the empty capsule and the much smaller difference for the closed capsule. Interestingly, both Bi@U_{24} and Pb@U_{24} exhibit a smaller R_g than the empty capsule, observed qualitatively in Figure 4 (by the shift of the slope to higher q values for Bi@U_{24} and Pb@U_{24} between q = 0.2–0.6 Å^{-1}) and quantitatively in Table 1. This finding nicely illustrates one difference between X-ray scattering and light scattering. The R_g value is the average of the squared center of the mass distances in the particle, weighted by the scattering length density. For the filled capsules, the center of mass is pulled inwards owing to the presence of the encapsulated heavy atoms.

For Pb@U_{24}, the experimental X-ray scattering curve also perfectly matches the simulated data to the first oscillation

peak at 0.8 $Å^{-1}$, and there is a clear difference between experimental and simulated $Pb@U_{24}$ and simulated empty U_{24}. However, the second and third oscillations are masked, likely owing to the disorder within the capsule as well as the solvent peak observed at about 2 $Å^{-1}$. Employing the IRENA macros within IGOR Pro,[18] we fitted the experimental and simulated data with a core–shell model (Table 1). The model parameters included the core radius and shell thickness and their electron scattering density. The fit of empty U_{24} indicates that the thicknesses of the core and shell are 3.6 Å and 4.4 Å, respectively, corresponding to a total diameter of 16 Å, which is consistent with the size observed in the solid-state structure. Fixing these core–shell dimensions, we fitted the experimental curves of $Bi@U_{24}$ and $Pb@U_{24}$ through refinement of the X-ray scattering length density (ρ) of the shell and the core. The ρ^{shell}/ρ^{core} ratio for $Li@U_{24}$ is very high compared to the ρ^{shell}/ρ^{core} ratios determined for $Bi@U_{24}$ and $Pb@U_{24}$, clearly indicating the filling of the uranyl capsule by metals with high electron density. Fourier transforms of the scattering data to obtain pair distance distribution functions (PDDFs, Figure SI5; described as a probability distribution map of scattering vectors through the cluster) for $Li@U_{24}$, $Pb@U_{24}$, and $Bi@U_{24}$ also show differences in the distribution of the scattering vectors inside the cluster while the overall size remains the same. This, too, is solely controlled by the nature of the encapsulated species.

Finally, both Raman spectroscopy (Figures S6–8) and electrospray ionization mass spectrometry (ESI-MS; Figure S9) indicated that cluster formation is essentially complete in two hours. These investigations also confirmed that $Pb@U_{24}$ and $Bi@U_{24}$ assemble far more rapidly than $Li@U_{24}$ from the triperoxide uranyl monomer.[5c]

In conclusion, we have described the encapsulation of metal oxo polycations inside uranyl peroxide polyanions. Similar host–guest chemistry has been described for polyoxometalates[19] and other metal oxo systems.[20] These were all obtained by trapping kinetic intermediates or by orchestrating the solution-phase compatibility between oftentimes very different chemistries. The synthesis and isolation of pure-phase $Pb@U_{24}$ and $Bi@U_{24}$ also overcame the challenge of combining aqueous clusters that are normally soluble and stable at opposite ends of the pH scale. In fact, $[Bi_6O_8]^{2+}$ and $[Pb_8O_6]^{4+}$ are poorly soluble in basic media, and their solubilization was only enabled by encapsulation in base-soluble U_{24}. The driving forces for the self-assembly are probably symmetry and size matching and electrostatic attraction between the polycation core and the polyanion shells. In turn, bismuth and lead accelerate the decomposition of peroxide, which speeds up cluster assembly. As most aqueous metal oxo polycations similarly self-assemble in acid, we anticipate that other known and unknown (e.g., $[Pb_8O_6]^{4+}$) metal oxo clusters can be encapsulated, leading to new discoveries in both polyoxocation and uranyl polyoxoanion chemistry. Finally, SAXS studies of the nested clusters highlighted the distinctive capabilities of this underutilized technique for characterizing aqueous cluster speciation.

Acknowledgements

We thank Dr. Lev Zakharov for help with single-crystal data collection and Dr. Stephen Huhn for help with ^{207}Pb NMR data collection. This work was supported as part of the Materials Science of Actinides, an Energy Frontier Research Center funded by the Department of Energy, Office of Science, Office of Basic Energy Sciences (DE-SC0001089).

Keywords: lone pair effects · nanocapsules · polyoxometalates · uranyl · X-ray diffraction

How to cite: *Angew. Chem. Int. Ed.* **2016**, *55*, 13480–13484
Angew. Chem. **2016**, *128*, 13678–13682

[1] a) M. T. Pope, A. Müller, *Angew. Chem. Int. Ed. Engl.* **1991**, *30*, 34–48; *Angew. Chem.* **1991**, *103*, 56–70; b) D. L. Long, E. Burkholder, L. Cronin, *Chem. Soc. Rev.* **2007**, *36*, 105; c) F. Secheresse, *Polyoxometalate Chemistry: Some Recent Trends*, *Vol. 8*, World Scientific, Singapore, **2013**.

[2] P. Yin, D. Li, T. Liu, *Chem. Soc. Rev.* **2012**, *41*, 7368–7383.

[3] P. C. Burns, K.-A. Kubatko, G. Sigmon, B. J. Fryer, J. E. Gagnon, M. R. Antonio, L. Soderholm, *Angew. Chem. Int. Ed.* **2005**, *44*, 2135–2139; *Angew. Chem.* **2005**, *117*, 2173–2177.

[4] a) M. Nyman, P. C. Burns, *Chem. Soc. Rev.* **2012**, *41*, 7354–7367; b) J. Qiu, P. C. Burns, *Chem. Rev.* **2013**, *113*, 1097–1120; c) J. Qiu, J. Ling, L. Jouffret, R. Thomas, J. E. S. Szymanowski, P. C. Burns, *Chem. Sci.* **2014**, *5*, 303–310.

[5] a) A. Gil, D. Karhánek, P. Miró, M. R. Antonio, M. Nyman, C. Bo, *Chem. Eur. J.* **2012**, *18*, 8340–8346; b) P. L. Zanonato, P. Di Bernardo, A. Fischer, I. Grenthe, *Dalton Trans.* **2013**, *42*, 10129–10137; c) Z. Liao, T. Deb, M. Nyman, *Inorg. Chem.* **2014**, *53*, 10506–10513; d) C. Falaise, M. Nyman, *Chem. Eur. J.* **2016**, DOI: 10.1002/chem.201602130; e) J. A. Soltis, C. M. Wallace, R. L. Penn, P. C. Burns, *J. Am. Chem. Soc.* **2016**, *138*, 191–198.

[6] a) E. M. Wylie, K. M. Peruski, J. L. Weidman, W. A. Phillip, P. C. Burns, *ACS Appl. Mater. Interfaces* **2014**, *6*, 473–479; b) F. Blanchard, M. Ellart, M. Rivenet, N. Vigier, I. Hablot, B. Morel, S. Grandjean, F. Abraham, *Chem. Commun.* **2016**, *52*, 3947–3950; c) E. M. Wylie, K. M. Peruski, S. E. Prizio, A. N. A. Bridges, T. S. Rudisill, D. T. Hobbs, W. A. Phillip, P. C. Burns, *J. Nucl. Mater.* **2016**, *473*, 125–130.

[7] a) P. Miró, S. Pierrefixe, M. Gicquel, A. Gil, C. Bo, *J. Am. Chem. Soc.* **2010**, *132*, 17787–17794; b) B. Vlaisavljevich, L. Gagliardi, P. C. Burns, *J. Am. Chem. Soc.* **2010**, *132*, 14503–14508; c) P. L. Zanonato, P. Di Bernardo, V. Vallet, Z. Szabo, I. Grenthe, *Dalton Trans.* **2015**, *44*, 1549–1556.

[8] a) F. Lazarini, *Acta Crystallogr. Sect. B* **1979**, *35*, 448–450; b) N. Henry, M. Evain, P. Deniard, S. Jobic, O. Mentré, F. Abraham, *J. Solid State Chem.* **2003**, *176*, 127–136; c) D. L. Rogow, H. Fei, D. P. Brennan, M. Ikehata, P. Y. Zavalij, A. G. Oliver, S. R. J. Oliver, *Inorg. Chem.* **2010**, *49*, 5619–5624; d) L. Miersch, T. Rüffer, M. Schlesinger, H. Lang, M. Mehring, *Inorg. Chem.* **2012**, *51*, 9376–9384.

[9] C. F. Baes, R. E. Mesmer, *Hydrolysis of cations*, Wiley, New York, **1976**.

[10] Crystallographic data for $Bi@U_{24}$: Tetragonal, $I4/m$, $a=b=19.0121(9)$, $c=25.7909(14)$ Å, $\alpha=\beta=\gamma=90°$, $V=9322.4(8)$ $Å^3$, $\rho_{calc}=3.451$ $g\,cm^{-3}$, $\mu(CuK_\alpha)=69.628$ cm^{-1}, 31481 reflections measured on an X8 Bruker CCD diffractometer at 173(2) K, $R1=0.0798$, $wR2=0.2032$, GOF = 1.075 for 4329 independent reflections with $I>2\sigma(I)$. Further details on the crystal structure investigations may be obtained from the Fachinformationszentrum Karlsruhe, 76344 Eggenstein-Leopoldshafen, Germany

(fax: (+49) 7247-808-666; e-mail: crysdata@fiz-karlsruhe.de), on quoting the depository number CSD-431616.
[11] T. A. Sullens, R. A. Jensen, T. Y. Shvareva, T. E. Albrecht-Schmitt, *J. Am. Chem. Soc.* **2004**, *126*, 2676 – 2677.
[12] Y. Wang, X. Yin, Y. Zhao, Y. Gao, L. Chen, Z. Liu, D. Sheng, J. Diwu, Z. Chai, T. E. Albrecht-Schmitt, S. Wang, *Inorg. Chem.* **2015**, *54*, 8449 – 8455.
[13] L. Shimoni-Livny, J. P. Glusker, C. W. Bock, *Inorg. Chem.* **1998**, *37*, 1853 – 1867.
[14] Crystallographic data for $Pb@U_{24}$: Cubic, $Im\bar{3}m$, $a=b=c=33.5330(6)$ Å, $\alpha=\beta=\gamma=90°$, $V=37706.6(12)$ Å^3, $\rho_{calc}=2.622\ g\,cm^{-3}$, $\mu(CuK_\alpha)=53.461\ cm^{-1}$, 120824 reflections measured on an X8 Bruker CCD diffractometer at 173(2) K, $R1=0.0821$, $wR2=0.1965$, GOF = 1.209 for 3218 independent reflections with $I>2\sigma(I)$. Depository number CSD-431617.
[15] P. C. Burns, *Am. Mineral.* **2000**, *85*, 801 – 805.
[16] P. Piret, J. Piret-Meunier, *Bull. Minéral.* **1988**, *111*, 439 – 442.
[17] T. M. Alam, Z. Liao, L. N. Zakharov, M. Nyman, *Chem. Eur. J.* **2014**, *20*, 8302 – 8307.
[18] J. Ilavsky, P. R. Jemian, *J. Appl. Crystallogr.* **2009**, *42*, 347 – 353.
[19] H. N. Miras, G. J. T. Cooper, D.-L. Long, H. Bögge, A. Müller, C. Streb, L. Cronin, *Science* **2010**, *327*, 72 – 74.
[20] M. Hervieu, B. Mellene, R. Retoux, S. Boudin, B. Raveau, *Nat. Mater.* **2004**, *3*, 269 – 273.

Received: July 23, 2016
Published online: September 27, 2016

